INTERNATIONAL JOURNAL FOR NUMERICAL METHODS IN FLUIDS, VOL. 22, 713–729 (1996)

THE NO-SLIP BOUNDARY CONDITION IN FINITE DIFFERENCE APPROXIMATIONS

HUAXIONG HUANG

Department of Mathematics and Statistics, Simon Fraser University, Burnaby, B.C., Canada V5A 1S6

AND

BRIAN R. SEYMOUR

Institute of Applied Mathematics, University of British Columbia, Vancouver, B.C., Canada V6T 1Z2

SUMMARY

A finite difference method for the Navier–Stokes equations in vorticity–streamfunction formulation is proposed to resolve the difficulty of the lack of a vorticity boundary condition at a no-slip boundary. It is particularly suitable for flows in regions with complicated geometries. Convergence with second-order accuracy in vorticity and velocity is established. In numerical experiments the convergence rates agree with theoretical predictions. Test results for the two-dimensional driven cavity problem and for the flow in expansion and contraction channels are given.

KEY WORDS: finite difference; boundary conditions; Navier–Stokes equations; convergence analysis

1. INTRODUCTION

The Navier–Stokes equations in streamfunction (ψ)-vorticity (ζ) variables can be written in the form

$$\zeta_t = -u\zeta_x - v\zeta_y + \frac{1}{Re}\Delta\zeta, \tag{1}$$

$$\zeta = -\Delta\psi, \tag{2}$$

$$u = \psi_y, \qquad v = -\psi_x \tag{3}$$

in a domain Ω, where u and v are the velocity components in directions x and y respectively and Re is the Reynolds number. The boundary conditions usually associated with a solid wall are

$$\psi = f, \tag{4}$$

$$\psi_n = g, \tag{5}$$

where n is the direction normal to the boundary.

One of the computational difficulties which arises in solving the coupled equations (1)–(3) is the lack of a vorticity condition at the solid wall. Although the use of discrete boundary conditions involving the (unspecified) vorticity on the wall has often been successful (e.g. Thom's formula[1] and its higher-order versions), direct implementation of the two natural conditions (4) and (5) is suggested as preferable by Gresho.[2] It is argued that specifying the vorticity on the boundary does not coincide with either physical or mathematical reality, since the boundary vorticity is related to the interior values by some global constraints. These are given explicitly in Reference 2, using the fact that the system of algebraic

CCC 0271–2091/96/080713-17

Received 17 June 1994
Revised 6 June 1995

equations obtained by discretizing equations (1)–(5) with an appropriate linearization has a unique solution. Another form of the global constraints is given in References 3–5.

Here we describe an approach that involves decoupling the boundary vorticity from the computation of the interior flow field. Then the vorticity values at the no-slip boundary are not needed to compute the streamfunction and vorticity values in the interior. One advantage of this approach is that the physical boundary conditions can be used directly. Also, flow fields that contain singularities in vorticity on the boundary (e.g. flows around sharp corners) can be calculated more readily, as the boundary vorticity is not computed explicitly. This approach has been applied successfully for various flow problems in References 6–9 and a similar method has been proposed by Napolitano.[10]

In Section 2 a description of the numerical method is given and a limited convergence analysis is outlined. The convergence analysis is based on discrete energy estimates, following Hou and Wetton.[11] The analysis is valid for problems with smooth solutions owing to the regularity requirement of the solution. The generalization to a general two-dimensional domain is given in Section 3. The results of numerical tests for a two-dimensional driven cavity and the flow in expansion and contraction channels are given in Section 4, including extensive comparisons with other methods.

2. FORMULATION AND CONVERGENCE ANALYSIS

For the convergence analysis we solve the coupled system (1)–(3) in a channel with a no-slip condition on the walls ($y = 0, 1$) and periodic conditions in the x-direction. Periodicity is used here to simplify the proof. The boundary conditions can be written in terms of the streamfunction as

$$\psi(x, 0; t) = \psi_0, \qquad \psi(x, 1; t) = \psi_1, \tag{6}$$

$$\psi_y(x, 0; t) = 0, \qquad \psi_y(x, 1; t) = 0, \tag{7}$$

where ψ_0 and ψ_1 are functions of x and t. Thus the boundary condition for ψ is overspecified, while no boundary condition is available for ζ. This difficulty is resolved by using the method presented here for the discrete finite difference approximation of (1)–(3). The semidiscrete equations are given now, followed by a convergence analysis.

2.1. *Semidiscrete equations*

The solution domain Ω is a 1×1 square which is covered by a uniform grid with spacing $h = 1/N$ and the discretized domain is denoted by $\Omega_h = \{(x_i, y_j), x_i = ih, y_j = jh; i, j = 0, \ldots, N\}$. Consider a spatial approximation $\tilde{\zeta}_{i,j}(t)$ to $\zeta(x_i, y_j; t)$. Approximations $\tilde{\psi}_{i,j}$, $\tilde{u}_{i,j}$ and $\tilde{v}_{i,j}$ are defined similarly. The difference operators that will be used are defined as

$$\begin{aligned} D_0^x f_{i,j} &= (f_{i+1,j} - f_{i=-1,j})/2h, \\ D_-^x f_{i,j} &= (f_{i,j} - f_{i-1,j})/h, \\ D_+^x f_{i,j} &= (f_{i+1,j} - f_{i,j})/h, \end{aligned} \tag{8}$$

with the operators D_0^y, D_-^y and D_+^y defined similarly. The difference Laplacian Δ_h is defined by centred differences as

$$\Delta_h = D_-^x D_+^x + D_-^y D_+^y.$$

The semidiscrete equations are now written as

$$\frac{\mathrm{d}}{\mathrm{d}t}\tilde{\zeta}_{i,j} = -\tilde{u}_{i,j}D_0^x\tilde{\zeta}_{i,j} - \tilde{v}_{i,j}D_0^y\tilde{\zeta}_{i,j} + \frac{1}{Re}\Delta_h\tilde{\zeta}_{i,j}, \tag{9}$$

$$\tilde{\zeta}_{i,j} = -\Delta_h\tilde{\psi}_{i,j}, \tag{10}$$

$$\tilde{u}_{i,j} = D_0^y\tilde{\psi}_{i,j}, \qquad \tilde{v}_{i,j} = -D_0^x\tilde{\psi}_{i,j}. \tag{11}$$

The no-slip conditions (6) and (7) can be discretized using an appropriate finite difference scheme. For example, a second-order approximation can be obtained as

$$\tilde{\psi}_{i,0} = \psi_0, \qquad \tilde{\psi}_{i,N} = \psi_1, \tag{12}$$

$$\tilde{\psi}_{i,1} = (\tilde{\psi}_{i,2} + 3\psi_0)/4, \qquad \tilde{\psi}_{i,N-1} = (\tilde{\psi}_{i,N-2} + 3\psi_1)/4. \tag{13}$$

The periodic boundary conditions are

$$\tilde{\psi}_{N,j} = \tilde{\psi}_{0,j}, \qquad \tilde{\zeta}_{N,j} = \tilde{\zeta}_{0,j}. \tag{14}$$

It can be seen that no vorticity conditions are explicitly used in the discretized no-slip conditions (12) and (13). The common practice is to derive an explicit condition for vorticity rather than using (12) and (13).

Following Reference 2, a numerical procedure can be designed such that the discretized no-slip conditions (12) and (13) are used directly. We first observe that in principle equations (9) and (10) can be solved consistently with the boundary conditions (12)–(14) by appropriate linearization. *No boundary conditions are needed for ζ at a no-slip wall.* We also observe that a constraint exists for the boundary value of ζ and equation (9) needs to be satisfied at $j = 1$ and $N - 1$ using the present discretization. Our final observation is that this constraint decouples from the rest of the system, as we can solve for ψ and ζ in the interior of Ω_h by a marching procedure for explicit time discretizations and an iterative procedure for implicit time discretizations or steady state computations. Since the two procedures are similar, we only discuss the iteration in the following.

We define the *computational domain*, $\Omega_h^c = \{(x_i, y_j),\ x_i = ih,\ y_j = jh;\ i = 0, \ldots, N, j = 1, \ldots, N - 1\}$, one grid inside Ω_h, the *physical domain*. The iterative procedure for solving (9) and (10) with an appropriate time discretization is now as follows.

1. Start the iteration by using equation (10) in the interior of Ω_h^c for $j = 2, \ldots, N - 2$ and $i = 0, \ldots, N - 1$. The streamfunction value ψ on $\partial\Omega_h^c$ at ($j = 1$ and $N - 1$) is obtained using both the no-slip boundary conditions (12) and (13) at the wall and the necessary conditions, periodic conditions in the present case, at the other boundaries. The resulting algebraic systems are solved using line Gauss–Siedel iteration.
2. Update u and v using the streamfunction value from step 1.
3. Condition (10), coupling ψ and ζ, is then satisfied on $\partial\Omega_h^c$ (at $j = 1$ and $N - 1$) and used to calculate ζ at those locations for $i = 0, \ldots, N - 1$.
4. The vorticity transport equation (9) is solved in the interior of Ω_h^c for $j = 2, \ldots, N - 2$ and $i = 0, \ldots, N - 1$ using the ζ-value on $\partial\Omega_h^c$ (at $j = 1$ and $N - 1$) from step 3 and the necessary conditions, periodic conditions in the present case, at the other boundaries. Again Gauss–Siedel iteration is used for the linearized algebraic system.
5. Steps 1–4 are repeated until convergence is reached.

The key to the success of this procedure is the fact that the ψ–ζ system is coupled. Note that we do not need to know the values of ζ at the no-slip walls, $j=0$ and N, to compute the interior values of ψ and ζ. This does not mean that the vorticity transport equation (9) is not satisfied at $j=1$ and $N-1$. The equation is satisfied in the sense that it provides a constraint for the ζ-values on the walls and this then provides an equation for finding the boundary values of ζ if we are interested in knowing them explicitly. Thus we can leave the vorticity value 'unknown' on a no-slip wall, with the understanding that its value is not arbitrary. A practical advantage of this procedure is that it can be applied to problems with sharp corners on the boundary, where the vorticity value is singular, as the explicit boundary vorticity value need not be displayed.

A similar idea, using the 'overspecified' streamfunction conditions directly, was used in Reference 10. However, here the streamfunction and vorticity are solved separately in the coupled discretized system instead of simultaneously. It should be mentioned that the idea of applying the streamfunction conditions (derived from the no-slip condition) is not new. Burggraf[12] introduced imaginary nodes outside the physical flow field in order to apply the streamfunction conditions directly. He then used the value of the streamfunction on the imaginary grids to compute the vorticity value on the boundary. This procedure is identical with the approach used by Thom[1] if the imaginary nodes are eliminated. In Reference 8 this technique was used in the computation of the flow in a constricted channel. Reasonable results were obtained despite the singularity in the vorticity at the corner.

There are two fundamental questions related to the numerical procedure just described that remain unanswered: the first concerns the optimal choice of parameters; the second concerns convergence. Usually, underrelaxation is necessary for step 4 to ensure convergence, with the relaxation parameter depending on the viscosity, grid size and time step size. However, no rigorous analysis is available for choosing the optimal parameter. For the linear limit of Stokes flow a rigorous analysis can be carried out by estimating the eigenvalues of the algebraic system and an optimal parameter can hence be calculated. We will not address this issue any further in this paper and the relaxation parameters used in our numerical tests are not optimal. Thus the issue of CPU will not be discussed when the numerical results are presented. Instead, we will focus our attention on the second question, i.e. whether the solution of the discrete system (9)–(14) converges to the solution of its continuous counterpart (1)–(3) with boundary conditions (6) and (7). In the following we will provide a rigorous analysis to show that a convergence of second order is established.

It is worth mentioning that second-order convergence is also proven for Thom's vorticity condition in Reference 11. However, the convergence results do not show which method is more accurate in terms of the actual size of the errors. Since the main difference between our proposed procedure and Burggraf's (Thom's) approach is the way in which Neumann condition for ψ is discretized (centred difference for Burggraf's approach and one-sided for ours), one can speculate that Burggraf's approach is more accurate owing to its smaller truncation error. However, we will not discuss this issue any further in this study. A comparison of various approaches to no-slip boundary conditions in terms of practical issues such as accuracy and efficiency is currently under way.

2.2. *Convergence analysis*

We first define the discrete norms on Ω_h^c:

$$\|f\|_2^2 = h^2 \sum_{i=0}^{N-1} \sum_{j=2}^{N-2} (f_{i,j})^2,$$

$$\|f\|_\infty = \max_i \max_{1 \leqslant j \leqslant N-1} |f_{i,j}|,$$

$$\|f\|_{1,2}^2 = h^2 \sum_{i=1}^{N} \sum_{j=2}^{N-1} [(D_-^x f_{i,j})^2 + (D_-^y f_{i,j})^2], \tag{15}$$

$$\|f\|_{2,2}^2 = h^2 \sum_{i=0}^{N-1} \sum_{j=2}^{N-2} (\Delta_h f_{i,j})^2.$$

The following relationships result from the definitions (15):

$$\|f\|_\infty \leqslant \frac{1}{h} \|f\|_2, \tag{16}$$

$$\|D_0^y f\|_2 \leqslant \|f\|_{1,2}, \tag{17}$$

$$\|f\|_2 \leqslant 3\|f\|_{1,2}, \tag{18}$$

where f satisfies $f_{i,0} = 0$, $f_{i,N} = 0$, $f_{i,2} = 4f_{i,1}$ and $f_{i,N-2} = 4f_{i,N-1}$. The inequality (16) holds simply because $h^2(f_{i,j})^2 \leqslant \|f\|_2^2$, while (18) is the discrete Poincaré inequality and follows from $f_{i,j} = h\sum_{1 \leqslant k \leqslant j} D_-^y f_{i,k}$, since $f_{i,0} = 0$ and $f_{i,j} = h\sum_{2 \leqslant k \leqslant j} D_-^y f_{i,k} + hD_-^y f_{i,1} = h\sum_{2 \leqslant k \leqslant j} D_-^y f_{i,k} + h/3D_-^y f_{i,2}$. The convergence results are given in the following theorem, with the assumption that the exact solution of the Navier–Stokes equations is sufficiently smooth.

Theorem 1

The solutions to the system (9)–(14) converge uniformly to the exact solutions to the Navier–Stokes equations with second-order accuracy:

$$\|\zeta - \tilde{\zeta}\|_\infty \leqslant C(T)h^2,$$

$$\|u - \tilde{u}\|_\infty \leqslant C(T)h^2, \qquad \|v - \tilde{v}\|_\infty \leqslant C(T)h^2,$$

for all t with $0 \leqslant t \leqslant T$.

To prove this theorem, some difficulties similar to those faced by Hou and Wetton[11] need to be overcome. First, Strang's argument[13] is generalized for the proof of consistency for the initial–boundary value problem in Lemma 1. The second lemma will give the stability bound for the proposed method and a combination of the two lemmas will lead to the proof of Theorem 1.

Lemma 1

There exists a smooth function $\hat{\psi}$ that is an $O(h^2)$ perturbation of ψ,

$$\hat{\psi}(x, y, t; h) = \psi(x, y, t) + \sum_{p=2}^{q-1} h_p \psi^{(p)}(x, y, t),$$

where the functions $\psi^{(p)}$ and their derivatives can be bounded in terms of ψ and its derivatives. It satisfies the no-slip and periodicity boundary conditions (12)–(19). Furthermore, $\hat{\zeta}_{i,j}$, which is defined to be $-\Delta_h \hat{\psi}_{i,j}$ in Ω_h^c, satisfies the discrete equations to any desired order of accuracy q as

$$\frac{\mathrm{d}}{\mathrm{d}t}\hat{\zeta}_{i,j} = -\hat{u}_{i,j} D_0^x \hat{\zeta}_{i,j} + \hat{v}_{i,j} D_0^y \hat{\zeta}_{i,j} + \frac{1}{Re}\Delta_h \hat{\zeta}_{i,j} + O(h^q), \tag{19}$$

$$\hat{u}_{i,j} = D_0^y \hat{\psi}_{i,j}, \qquad \hat{v}_{i,j} = -D_0^x \hat{\psi}_{i,j} \tag{20}$$

inside Ω_h^c, provided that the original solution ψ is smooth enough.

The boundary values of $\hat{\zeta}$ are not needed for computing its values on Ω_h^c; they can be obtained afterwards.

By defining the error terms as

$$\varepsilon_{i,j} = \tilde{\psi}_{i,j} - \hat{\psi}_{i,j}, \qquad e_{i,j} = \tilde{\zeta}_{i,j} - \hat{\zeta}_{i,j},$$

we have the second lemma.

Lemma 2

Given $T > 0$ and $\|\varepsilon(t)\|_{1,2} \leqslant h^{q-1/2}$ for $0 \leqslant t \leqslant T$, then there exists a positive number B depending only on T and the exact solution ζ such that for all t satisfying $0 \leqslant t \leqslant T$, provided that $q \geqslant 4$,

$$\frac{\mathrm{d}}{\mathrm{d}t}\|\varepsilon(t)\|_{1,2} \leqslant B(h^q + \|\varepsilon(t)\|_{1,2}). \tag{21}$$

Comments on the proofs of both lemmas are given in the Appendix. With these preparations we shall now prove the theorem.

Proof of Theorem 1

The theorem is proved in two steps.

1. First, Lemma 2 implies: given $T > 0$, we can find a $C(T)$ such that for all $0 \leqslant t \leqslant T$,

$$\|\varepsilon\|_{1,2} \leqslant C(T)h^q \tag{22}$$

for h small enough, where $C(T) - \mathrm{e}^{B(T)T}$. The proof of this can be found in Reference 11, with '$q - 2$' there replaced by '$q - \frac{1}{2}$'.

2. From (22) we have $\|\tilde{\psi} - \hat{\psi}\|_{1,2} \leqslant Ch^q$ (for $C \leqslant 1/2h^{1/2}$). Using (16), the relations

$$\max_{i,j} |D_-^x \tilde{\psi}_{i,j} - D_-^x \hat{\psi}_{i,j}| \leqslant \tfrac{1}{2} h^{q-1}$$

and

$$\max_{i,j} |D_-^y \tilde{\psi}_{i,j} - D_-^y \hat{\psi}_{i,j}| \leqslant \tfrac{1}{2} h^{q-1}$$

hold for $i, j = 1, \ldots, N-1$. Because $\tilde{\zeta}_{i,j} = -\Delta_h \tilde{\psi}_{i,j} = -(D_+^x D_-^x + D_+^y D_-^y)\tilde{\psi}_{i,j}$, thus

$$\max_{i,j} |\tilde{\zeta}_{i,j} - \Delta_h \hat{\psi}_{i,j}| \leqslant \tfrac{1}{2} h^{q-2} \tag{23}$$

on Ω_h^c. From Lemma 1, $\Delta_h \hat{\psi}_{i,j} = (\Delta\psi)_{i,j} + O(h^2) = -\zeta_{i,j} + O(h^2)$. By choosing $q \geqslant 4$, the combination of Lemma 1 and (23) gives uniform second-order convergence for the vorticity in Ω_h^c and the convergence for the velocity components is obtained similarly.

3. GENERALIZATION TO OTHER DOMAINS

Although the convergence proof in the previous section is given for a periodic channel flow problem, it is noted that this is a choice of convenience rather than a restriction. It is also noted that the analysis is not restricted to two space dimensions. An analysis for three space dimensions and other domains was given for Thom's method by Hou and Wetton.[11] As the only difference between the present analysis and that in Reference 11 is in the estimates of boundary terms, we could prove the convergence using the

same procedures with our boundary estimate. For the purpose of conciseness, only the analysis of a general two-dimensional domain is given in the following.

Here we consider the situation where a curvilinear co-ordinate system $(\xi(x, y), \eta(x, y))$ can be set up to conformally map the irregular domain Ω_* onto the periodic channel. Following Reference 11, the transformed equations are

$$\frac{1}{J}\zeta_t + u\zeta_\xi + v\zeta_\zeta = \frac{1}{Re}\tilde{\Delta}\zeta, \tag{24}$$

$$J\tilde{\Delta}\psi = -\zeta, \tag{25}$$

$$u = \psi_\eta, \qquad v = -\psi_\xi, \tag{26}$$

where $J = |(\partial\xi, \partial\eta)/(\partial x, \partial y)|$ is the Jacobian and $\Delta = J\tilde{\Delta} = J(\partial^2/\partial\xi^2 + \partial^2/\partial\eta^2)$. The boundary conditions are

$$\psi(\xi, 0; t) = \psi_0, \qquad \psi(\xi, 1; t) = \psi_1, \tag{27}$$

$$\psi_\eta(\xi, 0; t) = 0, \qquad \psi_\eta(\xi, 1; t) = 0, \tag{28}$$

with periodicity in the ξ-direction. The semidiscrete equations are

$$\frac{1}{J_{i,j}}\frac{\mathrm{d}}{\mathrm{d}t}\tilde{\zeta}_{i,j} = -\tilde{u}_{i,j}D_0^x\tilde{\zeta}_{i,j} + \tilde{v}_{i,j}D_0^y\tilde{\zeta}_{i,j} + \frac{1}{Re}\tilde{\Delta}_h\tilde{\zeta}_{i,j}, \tag{29}$$

$$J_{i,j}\tilde{\Delta}_h\tilde{\psi}_{i,j} = -\tilde{\zeta}_{i,j}, \tag{30}$$

$$\tilde{u}_{i,j} = D_0^y\tilde{\psi}_{i,j}, \qquad \tilde{v}_{i,j} = -D_0^x\tilde{\psi}_{i,j}. \tag{31}$$

The boundary conditions are

$$\tilde{\psi}_{i,0} = \psi_0, \qquad \tilde{\psi}_{i,N} = \psi_1, \tag{32}$$

$$\tilde{\psi}_{i,1} = (\tilde{\psi}_{i,2} + 3\psi_0)/4, \qquad \tilde{\psi}_{i,N-1} = (\tilde{\psi}_{i,N-2} + 3\psi_1)/4 \tag{33}$$

at a no-slip wall. The periodic boundary conditions are

$$\tilde{\psi}_{N,j} = \tilde{\psi}_{0,j}, \qquad \tilde{\zeta}_{N,j} = \tilde{\zeta}_{0,j}. \tag{34}$$

With the assumption of smooth J, the equivalent convergence result to Theorem 1 again follows. Notice that (29)–(34) has a similar structure to (9)–(14) with the smooth positive weights $J_{i,j}$. This allows us to prove the equivalents of Lemmas 1 and 2 in a similar way.

4. NUMERICAL TESTS

We have established convergence of the finite difference equations for flow in a periodic channel (and regions that can be mapped onto a periodic channel) in the previous sections. While the solution must remain sufficiently smooth for the convergence analysis to hold, it is still possible to use the approach for other, more practical, problems. In this section we provide numerical evidence to show that the method can be applied to several problems with sharp corners, even though no theoretical results are available. Second-order convergence is still evident when the solutions are relatively smooth.

Numerical experiments were performed with uniform grids using the methods described in the previous section for flows in a driven cavity and in expansion and contraction channels. The numerical accuracy is assessed through comparison with previously reported results. The numerical tests are

Table I. Driven cavity: comparison of streamfunction and vorticity values at centre of primary and secondary vortices

		Primary vortex		Secondary vortex left		Secondary vortex right	
Re	Source	ψ	ζ	ψ	ζ	ψ	ζ
100	Present	0·10336	3·16500	1·39(−6)	0·0141	9·96(−6)	0·0328
	Ghia *et al.*	0·10342	3·16646	1·75(−6)	0·0156	1·25(−5)	0·0331
	Schreiber and Keller	0·10330	3·18200	2·05(−6)	0·0080	1·32(−5)	0·0255
1000	Present	0·11668	2·02904	2·14(−4)	0·3566	1·63(−3)	1·0304
	Ghia *et al.*	0·11793	2·04968	2·31(−4)	0·3618	1·75(−3)	1·1547
	Schreiber and Keller	0·11603	2·02600	2·17(−4)	0·3020	1·70(−3)	0·9990
5000	Present	0·11621	1·83445	1·30(−3)	1·3330	2·68(−3)	2·5311
	Ghia *et al.*	0·11897	1·86016	1·36(−3)	1·5306	3·08(−3)	2·6635
	Schreiber and Keller	—	—	—	—	—	—
10,000	Present	0·11286	1·74198	1·57(−3)	1·8611	2·66(−3)	2·8615
	Ghia *et al.*	0·11973	1·88082	1·52(−3)	2·0856	3·42(−3)	4·0531
	Schreiber and Keller	0·10284	1·62200	1·12(−3)	1·0670	2·96(−3)	3·0310

carried out for steady state solutions only; ζ_t is kept as a relaxation term and t loses its physical meaning and acts as a pure relaxation parameter. The discretized governing equations are solved following the iterative procedure described in Section 2. Centred differences are used unless specified otherwise.

4.1. Two-dimensional driven cavity problem

The flow in a driven cavity is used as the first test problem. The fluid is confined in a 1×1 square cavity driven by the top wall moving with velocity $u = 1$, while the other walls are at rest. This problem is recognized as a standard test case for assessing the efficiency and accuracy of the numerical simulation of the Navier–Stokes equations. This is because it contains some general characteristics such as recirculation, while the geometry and boundary conditions are relatively simple and well-defined. Extensive results have been published on the subject in the last 10 years.

The computations in this case were carried out for $Re = 100$, 1000, 5000 and 10,000 with a 129×129 grid for a direct comparison with the results of Ghia *et al.*[14] and Schreiber and Keller.[15] Table I shows that the present results for the primary vortex and minimum streamfunction have at least two or three digits in agreement with most of the results obtained by previous investigators. The velocity components along the vertical and horizontal lines through the cavity centre are presented in Tables II(a) and II(b) respectively for $Re = 1000$, 5000 and 10,000. They also show reasonably good agreement. It can be seen from Table I that the vorticity results start to show some discrepancy between the present prediction and those by Ghia *et al.*[14] and others[15] for $Re \geqslant 5000$, especially for the secondary vortices. This indicates that the accuracy at high Reynolds number is still an open question, because the corner singularities result in a large gradient of vorticity near the wall.

The calculations were also completed for 61×61, 81×81 and 101×101 grids at $Re = 100$ and 1000 to assess the convergence rate α. An analytical solution in this case is not available. Thus the convergence rate is calculated using three different grid sizes h_1, h_2 and h_3 as

$$\alpha = \frac{F_{c2} - F_{c1}}{F_{c3} - F_{c1}} = \frac{h_2^\alpha - h_1^\alpha}{h_3^\alpha - h_1^\alpha}. \tag{35}$$

Table II. Driven cavity: (a) comparison of u-velocity component along vertical line through cavity centre; (b) comparison of v-velocity component along horizontal line through cavity centre

(a)		$Re = 1000$		$Re = 5000$		$Re = 10{,}000$	
Grid point	y-Location	Present	Ghia *et al.*	Present	Ghia *et al.*	Present	Ghia *et al.*
129	1·0000	1·0000	1·0000	1·0000	1·0000	1·0000	1·0000
126	0·9766	0·6590	0·6593	0·4719	0·4822	0·4442	0·4722
125	0·9688	0·5749	0·5749	0·4499	0·4612	0·4510	0·4778
124	0·9609	0·5133	0·5112	0·4491	0·4599	0·4540	0·4807
123	0·9531	0·4663	0·4660	0·4502	0·4604	0·4515	0·4780
110	0·8516	0·3324	0·3330	0·3306	0·3356	0·3198	0·3464
95	0·7344	0·1063	0·1872	0·1941	0·2009	0·1906	0·2067
80	0·6172	0·0563	0·0570	0·0775	0·0818	0·0797	0·0834
65	0·5000	−0·0613	−0·0608	−0·0295	−0·0304	−0·0223	−0·0311
59	0·4531	−0·1068	−0·1065	−0·0711	−0·0740	−0·0621	−0·0754
37	0·2813	−0·2777	−0·2781	−0·2223	−0·2286	−0·2078	−0·2319
23	0·1719	−0·3826	−0·3829	−0·3212	−0·3305	−0·3035	−0·3271
14	0·1016	−0·2953	−0·2973	−0·3996	−0·4044	−0·3684	−0·3800
10	0·0703	−0·2199	−0·2222	−0·4246	−0·4364	−0·4121	−0·4166
9	0·0625	−0·1998	−0·2020	−0·4154	−0·4290	−0·4245	−0·4254
8	0·0547	−0·1791	−0·1811	−0·3971	−0·4117	−0·4312	−0·4274
1	0·0000	0·0000	0·0000	0·0000	0·0000	0·0000	0·0000
(b)		$Re = 1000$		$Re = 5000$		$Re = 10{,}000$	
Grid point	x-Location	Present	Ghia *et al.*	Present	Ghia *et al.*	Present	Ghia *et al.*
129	1·0000	0·0000	0·0000	0·0000	0·0000	0·0000	0·0000
125	0·9688	−0·2273	−0·2139	−0·5105	−0·4977	−0·5481	−0·5430
124	0·9609	−0·2910	−0·2767	−0·5489	−0·5507	−0·5121	−0·5299
123	0·9531	−0·3514	−0·3371	−0·5434	−0·5541	−0·4732	−0·4910
122	0·9453	−0·4054	−0·3919	−0·5152	−0·5288	−0·4474	−0·4586
117	0·9063	−0·5192	−0·5155	−0·4098	−0·4144	−0·3963	−0·4150
111	0·8594	−0·4215	−0·4267	−0·3568	−0·3621	−0·3396	−0·3674
104	0·8047	−0·3159	−0·3197	−0·2928	−0·3002	−0·2778	−0·3072
65	0·5000	0·0265	0·0253	0·0147	0·0095	0·0151	0·0081
31	0·2344	0·3222	0·3224	0·2690	0·2728	0·2535	0·2722
30	0·2266	0·3306	0·3308	0·2768	0·2807	0·2608	0·2800
21	0·1563	0·3707	0·3710	0·3488	0·3537	0·3276	0·3507
13	0·0938	0·3261	0·3263	0·4175	0·4295	0·3934	0·4149
11	0·0781	0·3032	0·3035	0·4194	0·4365	0·4116	0·4312
10	0·0703	0·2897	0·2901	0·4135	0·4333	0·4177	0·4373
9	0·0625	0·2742	0·2749	0·4023	0·4245	0·4190	0·4398
1	0·0000	0·0000	0·0000	0·0000	0·0000	0·0000	0·0000

F_{c1}, F_{c2} and F_{c3} are numerical solutions for grid sizes h_1, h_2 and h_3 respectively and are evaluated on the same grid point. Table III presents the convergence rates for the sequence of solutions that approach the actual solution. It can be seen that the computed convergence rates for both vorticity (α_ζ) and streamfunction (α_ψ) values are below the value two, which is the theoretical value for convergence of second order, although they approach two when the grids are refined. This shows that second-order convergence is not reached on all grids tested. The reason is that the vorticity is singular at corners and this singularity contaminates the overall solutions. A similar test using a smoother velocity profile

Table III. Convergence rate test of solutions of driven cavity flow

Grid numbers	Re	α_ψ	α_ζ
40–60–80	100	1·213	1·642
60–80–100	100	1·421	1·685
80–100–120	100	1·555	1·707

Table IV. Convergence rate test of solutions of driven cavity flow with smooth velocity profile $u = x^2(1-x)^2$ at driven wall

Grid numbers	Re	α_ψ	α_ζ
40–60–80	100	1·954	1·913
60–80–100	100	2·126	1·938

$u = x^2(1-x)^2$ at the driven wall shows that the second-order convergence rate is reached for both streamfunction and vorticity values (Table IV).

The streamline plots in Figure 1 show the development of a central, nearly circular vortex with bottom secondary vortices. For $Re = 5000$ a third secondary vortex near the top left corner is present, while for $Re = 10{,}000$ a tertiary vortex in the bottom right region appears. This is consistent with the results of Ghia *et al.*[14] The contour plots in Figure 2 show a centre region of essentially constant vorticity surrounded by a nearly circular, thin region of highly oscillatory vorticity. Mesh frequency oscillations near the downstream top corner are evident at $Re = 5000$, earlier than those observed by Ghia *et al.*,[14] since a coarser grid is used in the present computation. This is expected, as the mesh with centred differences is not sufficiently fine to resolve the boundary layer.

4.2. Flow in an expansion channel

The flow in an expansion channel was chosen by the organizers of a GAMM workshop as a standard test case for comparing the performance of codes for solving the incompressible Navier–Stokes equations[16] because of its simple geometry. The flow in an expansion channel proves to be a good test case also because of its interesting features. All codes produce a vortex at the same separation point and the prediction of the position of reattachment then presents a challenge for the performance of any numerical algorithm. As pointed out by Morrison and Napolitano,[17] most methods face convergence difficulties when $Re > 500$. This is because the flow structure becomes more complicated physically when Re increases, as shown clearly by the careful experiments of Armaly *et al.*[18] Another challenge presented by this problem is the downstream flow condition. Proper outflow conditions must be provided to ensure the convergence of the solution procedure. Morgan *et al.*[16] have discussed this point in detail.

In the present study, results are obtained for a step size equal to half the height of the channel, which is assumed to be 2. The length of the channel is chosen to be 30. Let L_1 be the horizontal distance between the reattachment point of the primary vortex at the lower wall and the step (where the separation occurs). There is also a secondary vortex at the top wall when the Reynolds number increases. Let L_2 be the separation point of the secondary vortex and L_3 the reattachment point of the secondary vortex at the top wall.

The computation was carried out on a uniform 201×101 grid over a 15×1 domain. Figure 3 present contours of the streamfunction for $Re = 200$, 400, 600 and 800. It can be seen that the size of the recirculation region increases with the Reynolds number. At $Re = 600$ and above a secondary vortex

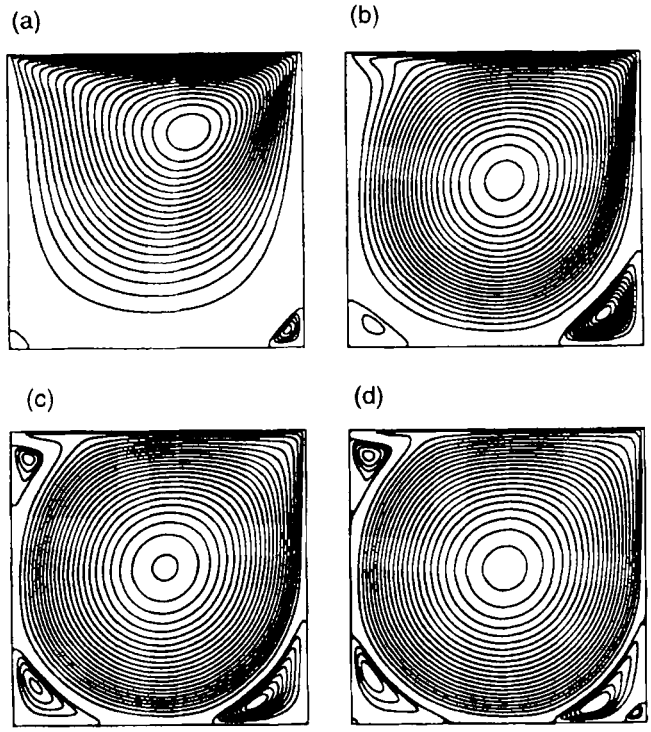

Figure 1. Streamline contours for driven cavity flow: (a) $Re = 100$; (b) $Re = 1000$; (c) $Re = 5000$; (d) $Re = 10{,}000$

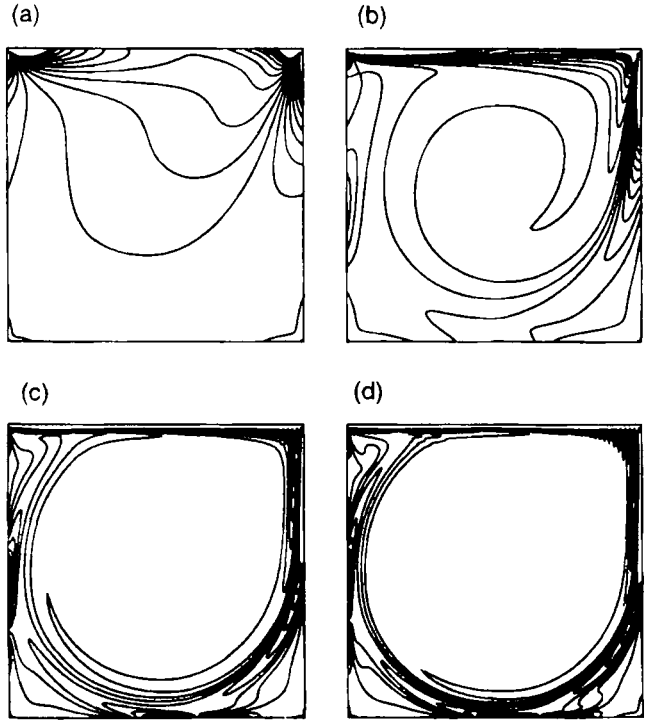

Figure 2. Vorticity contours for driven cavity flow: (a) $Re = 100$; (b) $Re = 1000$; (c) $Re = 5000$; (d) $Re = 10{,}000$

Table V. Comparison of separation and reattachment points for flow in expansion channel

	Armaly *et al.*			Morrison and Napolitano			Present		
Re	L_1	L_2	L_3	L_1	L_2	L_3	L_1	L_2	L_3
200	—	—	—	5·3	—	—	5·4	—	—
400	8·6	—	—	8·6	8·0	10·4	8·7	8·0	10·4
600	11·5	—	—	10·7	8·7	16·2	10·8	8·8	16·2
800	14·3	—	—	12·2	9·7	21·0	12·3	9·8	21·0

develops at the top wall. Second-order accuracy was obtained by setting the parameter $\alpha_{i,j} = \Delta y$ using the single-step upwind scheme.[19] Table V presents a comparison of the separation and reattachment points L_i between the present calculation and the results of Armaly *et al.*[18] and Morrison and Napolitano.[17] The agreement is reasonably good between the two numerical predictions. A possible reason for the discrepancy at $Re = 800$ between the experiment and the numerical results may be the instability of the flow when the Reynolds number becomes large, as mentioned in Reference 18.

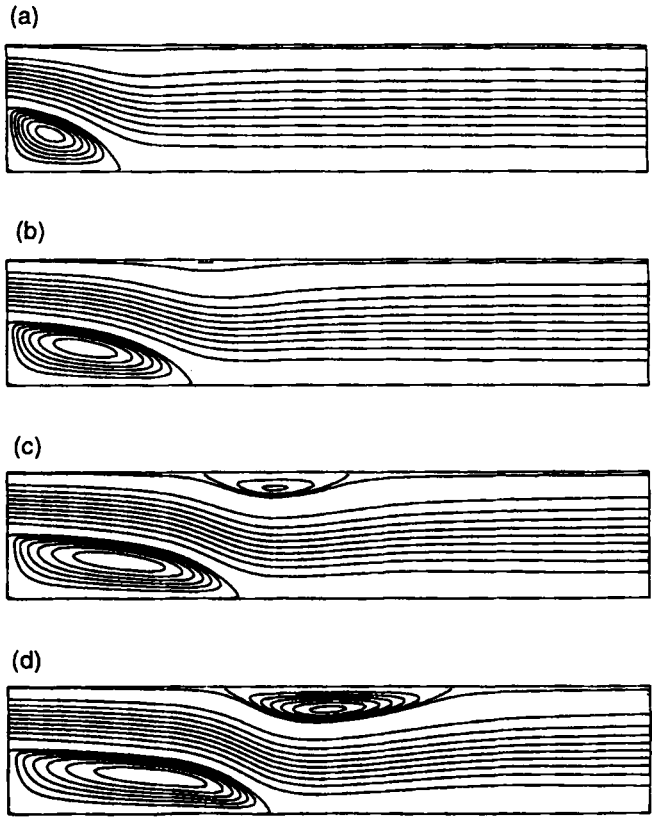

Figure 3. Streamline contours for flow in expansion channel: (a) $Re = 200$; (b) $Re = 400$; (c) $Re = 600$; (d) $Re = 800$

Table VI. Reattachment point of tip corner vortex measured from corner ($Re = 500$)

Dennis and Smith	Not detected
Hawken *et al.*	0·440
Karageorghis and Phillips	0·995
Present (transformation)	0·430
Present (Cartesian)	0·444
Burggraf's method	0·415

4.3. Flow in a contraction channel

Flow in a contraction channel is a more difficult test problem in the sense that the separation after the contraction is difficult to compute accurately, as shown in Reference 8. Although vorticity singularities are present in the driven cavity and expansion channel, one does not need to deal with them explicitly using the finite difference approximation, since the corner values are not needed for computation. In the contraction channel, however, the vorticity value at the tip corner is needed using a conventional approach. Special techniques have to be used to estimate the vorticity values near the corner,[20] while some investigators took a semianalytical approach by using the local solutions obtained in Reference 21. Our solution procedure does not need the vorticity values on the solid wall, which makes it more readily applicable to this and similar problems. We refer interested readers to Reference 8 for a detailed discussion. Only a typical test case is cited here. The channel width is assumed to be 2 before the step and 1 after the step. The lengths are 2 before and after the step. The computation is only carried out on half the channel because of the symmetry.

Figure 4 shows the streamline contours for $Re = 500$ (based on the channel width before the step.) Separation regions before and after the step are apparent. Most of the previous investigators in the literature were able to predict the separation before the step reasonably well. However, large discrepancies exist in the predictions of the separation region after the tip corner. Table VI presents the results of the computed reattachment point for the tip corner separation. The first three rows are the results from previous investigations. Large discrepancies are apparent. Our numerical results using both a Cartesian grid and a transformation are consistent and close to that of Hawken *et al.*,[22] where a primitive variable formulation is used so that the explicit treatment of the vorticity singularity is avoided.

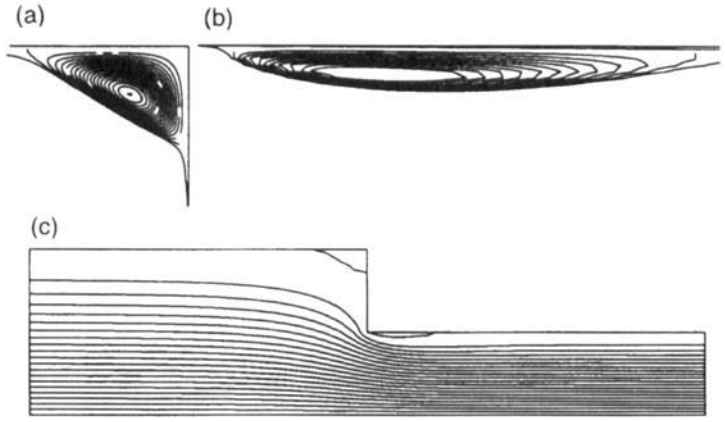

Figure 4. Streamline contours for flow in contraction channel ($Re = 500$): (a) close-up view at salient corner; (b) close-up view of separation after tip corner; (c) overall view

The prediction using Burggraff's imaginary cell is somewhat lower, but much closer to those of ours than that of Karageorghis and Phillips,[23] where a spectral element method was used.

5. CONCLUSIONS

A method for resolving the lack of an appropriate vorticity boundary condition at a solid wall for certain finite difference algorithms has been presented, together with a convergence analysis for simplified situations. The structure of the convergence proof is similar to that of Hou and Wetton[11] for Thom's first-order vorticity boundary condition.

Accurate numerical results are obtained for several test problems and these are compared with many previous results. The numerical experiments also confirmed the second-order accuracy predicted by the convergence analysis. Although the numerical experiments are carried out for two-dimensional problems with simple geometries, the method is suitable for solving problems with more complex geometries. Successful calculations have been carried out for flows in irregular geometries, such as blood flow in constricted arteries.[7] The method is particularly suitable for problems with corner singularities and the results are in good agreement with those using other methods.[8]

ACKNOWLEDGEMENT

The authors wish to thank Dr. Brian Wetton for his helpful suggestions.

APPENDIX

Since the proofs of both lemmas are similar to those in Reference 11, we will only describe briefly the structure of our proofs. Interested readers are referred to Reference 11.

Comments on proof of Lemma 1

This lemma is proven in a constructive way, i.e. an approximate solution $\tilde{\psi}(x, y, t; h)$ is constructed such that it satisfies Lemma 1. To construct an approximation to the exact solution $\psi(x, y, t)$ of order q, we consider an expansion similar to Strang:[13]

$$\tilde{\psi}(x, y, t; h) = \sum_{p=0}^{q-1} h^p \psi^{(p)}(x, y, t). \tag{36}$$

The procedure to determine each function $\psi^{(p)}$ is the same as in Reference 11, by considering the interior and boundary conditions separately.

Equations for $\psi^{(p)}$. It is expected from Lemma 1 that $\tilde{\psi}$ will satisfy equation (19). By rearranging the equation according to the order of h, a series of equations is obtained for each function $\psi^{(p)}$. For example, a pth-order equation is

$$h^p: \quad \frac{\partial}{\partial t}\Delta\psi^{(p)} = -\psi_y^{(0)}\Delta\psi_x^{(p)} + \psi_x^{(0)}\Delta\psi_y^{(p)} + \frac{1}{Re}\Delta^2\psi(p) - \psi_y^{(p)}X^{(p)} + \psi_x^{(p)}Y^{(p)} + F^{(p)}, \tag{37}$$

where $X^{(p)}$, $Y^{(p)}$ and $F^{(p)}$ are linear combinations of $\psi^{(r)}$ with $r < p$.

Boundary conditions for $\psi^{(p)}$. The boundary conditions for $\tilde{\psi}$ are the physical conditions (e.g. at $y = 0$):

$$4\hat{\psi}_{i,1} - \hat{\psi}_{i,2} - 3\hat{\psi}_{i,0} = 0. \tag{38}$$

An expression in continuous form can be obtained using a Taylor expansion as

$$\frac{\partial \hat{\psi}_{i,0}}{\partial y} + \cdots + 2(1 - 2^{p-2}) \frac{h^{p-1}}{p!} \frac{\partial^p \hat{\psi}_{i,0}}{\partial y^p} = 0. \tag{39}$$

Inserting equation (36) into equations (38) and (39) and rearranging the terms yields boundary conditions. For example, the pth-order boundary conditions are

$$h^p: \quad \psi^{(p)} = 0, \qquad \psi_y^{(p)} = -2(1 - 2^{p-2}) \frac{\psi_y^{(p-2)}}{p!} + \cdots. \tag{40}$$

Similar boundary conditions are derived at $y = 1$, while the periodic condition will be valid for each function $\psi^{(p)}$ in the x-direction, i.e. $x = 0$ and 1.

Discussion of solution $\psi^{(p)}$. The system of equations for $\psi^{(p)}$ can be solved inductively from $p = 0$ to any desired order $p = q$. The equation and boundary conditions for the zeroth order ($\psi^{(0)}$) are identical with the original Navier–Stokes equations. Thus $\psi^{(0)} = \psi$. The boundary condition for the first-order functin $\psi^{(1)}$ is homogeneous, so the solution is $\psi^{(1)} = 0$. This is as we expected, since the exact solution should not contain the first-order correction. If all the compatibility conditions for initial data are satisfied to ensure the smoothness of the solution at $t = 0$, the expansion ψ has the properties required in Lemma 1.

Comments on proof of Lemma 2

The proof of Lemma 2 is carried out by providing a bound for the discrete energy. Only the homogeneous boundary conditions are considered, since the non-homogeneous case can be proved similarly. Subtracting equation (9) from equation (19) on Ω_h^c, we obtain

$$\frac{\mathrm{d}e_{i,j}}{\mathrm{d}t} = \tag{41}$$

$$- D_0^y \varepsilon_{i,j} \cdot D_0^x e_{i,j} \tag{42}$$

$$+ D_0^y \varepsilon_{i,j} \cdot D_0^x \Delta_h \hat{\psi}_{i,j} \tag{43}$$

$$- D_0^y \hat{\psi}_{i,j} \cdot D_0^x e_{i,j} \tag{44}$$

$$- D_0^x \varepsilon_{i,j} \cdot D_0^y e_{i,j} \tag{45}$$

$$+ D_0^x \varepsilon_{i,j} \cdot D_0^y \Delta_h \hat{\psi}_{i,j} \tag{46}$$

$$- D_0^x \hat{\psi}_{i,j} \cdot D_0^y e_{i,j} \tag{47}$$

$$+ \frac{1}{Re} \Delta_h e_{i,j} \tag{48}$$

$$+ O(h^q). \tag{49}$$

The terms (41)–(49) are multiplied by $h^2\varepsilon_{i,j}$ and summed over Ω_h^c. Then, using summation by parts and the boundary conditions for ε, they are evaluated term-by-term using $\varepsilon_{i,0} = \varepsilon_{i,N} = 0$, $\varepsilon_{i,2} = 4\varepsilon_{i,1}$, $\varepsilon_{i,N-1} = 4\varepsilon_{i,N-1}$ and the two identities

$$\sum_{j=2}^{N-2} f_j D_+ g_j = -\sum_{j=2}^{N-2} g_j D_- f_j + \tfrac{1}{h}(f_{N-2}g_{N-1} - f_1 g_2) \tag{50}$$

$$= -\sum_{j=2}^{N-1} g_j D_- f_j + \tfrac{1}{h}(f_{N-1}g_{N-1} - f_1 g_2) \tag{51}$$

and

$$\sum_{j=2}^{N-2} f_j D_- g_j = -\sum_{j=2}^{N-2} g_j D_+ f_j + \tfrac{1}{h}(f_{N-1}g_{N-2} - f_2 g_1). \tag{52}$$

Again the procedure is similar to that in Reference 11. The difference arises from the estimates of the boundary terms but can be estimated in a similar fashion. We will present the estimates for each term without detailed derivation and refer interested readers to Reference 11.

Firstly we have

$$(41) \geqslant \frac{1}{2}\frac{\mathrm{d}}{\mathrm{d}t}\|\varepsilon\|_{1,2}^2 \tag{53}$$

instead of an equal sign in Reference 11. The estimates for the non-linear terms (42) and (45) are much simpler here, since no boundary terms appear using our boundary condition. The interior terms are bounded by brute force $\|\varepsilon\|_{1,2} \leqslant h^q$ for $0 \leqslant t \leqslant T$ as

$$(42), (45) \leqslant K\|\varepsilon\|_{1,2}^2 \tag{54}$$

by using the Cauchy–Schwarz inequality, where K is a constant. The linearized convection terms are bounded owing to the fact that $D_0^x \Delta_h \hat{\psi}_{i,j}$ is bounded. Since the boundary terms do not appear, the estimates for (43) and (46) are the same as in Reference 11:

$$(43), (46) \leqslant K\|\varepsilon\|_{1,2}^2. \tag{55}$$

The estimates for (44) and (47) are the most cumbersome, as it is necessary to evaluate some of the boundary terms. After lengthy manipulation and the use of the boundary condition we obtain

$$(44), (47) \leqslant K\|\varepsilon\|_{1,2}^2. \tag{56}$$

The diffusion term is evaluated assuming $Re = 1$ for convenience:

$$(48) = -\|\varepsilon\|_{2,2}^2. \tag{57}$$

Finally,

$$(49) \leqslant O(h^q)\|\varepsilon\|_{1,2}. \tag{58}$$

Combining these yields

$$\begin{aligned} \frac{1}{2}\frac{\mathrm{d}}{\mathrm{d}t}\|\varepsilon\|_{1,2}^2 &\leqslant -\frac{1}{Re}\|\varepsilon\|_{2,2}^2 + K\|\varepsilon\|_{1,2}^2 + O(h^q)\|\varepsilon\|_{1,2} \\ &\leqslant B\|\varepsilon\|_{1,2}(h^q + \|\varepsilon\|_{1,2}) \end{aligned} \tag{59}$$

or

$$\frac{\mathrm{d}}{\mathrm{d}t}\|\varepsilon\|_{1,2} \leqslant B(h^q + \|\varepsilon\|_{1,2}). \tag{60}$$

REFERENCES

1. A. Thom, 'The flow past circular cylinder at low speeds', *Proc. R. Soc. Lond. A*, **141**, 651–666 (1933).
2. P. M. Gresho, 'Incompressible fluid dynamics: some fundamental formulation issues', *Ann. Rev. Fluid Mech.*, **23**, 413–453 (1991).
3. L. Quartapelle, 'Vorticity condition in the computation of two-dimensional viscous flows', *J. Comput. Phys.*, **40**, 453 (1981).
4. F. V. Valz-Gris and L. Quartapelle, 'Projection conditions on the vorticity in viscous incompressible flows', *Int. j. numer. methods fluids*, **1**, 453 (1981).
5. S. C. R. Dennis and L. Quartapelle, 'Some uses of Green's theorem in solving the Navier–Stokes equations', *Int. j. numer. methods fluids*, **9**, 871–890 (1989).
6. H. Huang, 'Incompressible viscous flow in tubes with occlusions', *Ph.D. Dissertation*, University of British Columbia, 1992.
7. H. Huang, B. R. Seymour and V. J. Modi, 'A new finite difference method and its application in flows of stenosed arteries', *Contemp. Math.*, **141**, 337–350 (1991).
8. H. Huang and B. R. Seymour, 'A finite difference method for flow in a constricted channel', *Comput. Fluids*, **24**, 153–160 (1995).
9. M. Li, T. Tang and B. Fornberg, 'A compact fourth order finite difference scheme for the steady incompressible Navier–Stokes equations', *Int. j. numer. methods fluids*, **20**, 1137–1151 (1995).
10. M. Napolitano, 'Efficient solution of two-dimensional steady separated flows', *Comput. Fluids*, **20**, 213–222 (1991).
11. T. Y. Hou and B. T. R. Wetton, 'Convergence of a finite difference scheme for the Navier–Stokes equations using vorticity boundary conditions', *SIAM J. Numer. Anal.*, **29**, 615–639 (1992).
12. O. R. Burggraf, 'Analytical and numerical studies of the structure of steady separated flows', *J. Fluid Mech.*, **24**, 113–151 (1966).
13. G. Strang, 'Accurate partial differential methods II. Non-linear problems', *Numer. Math.*, **6**, 37–46 (1964).
14. U. Ghia, K. N. Ghia and C. T. Shin, 'High-Re solutions for incompressible flow using the Navier–Stokes equations and a multigrid method', *J. Comput. Phys.*, **48**, 387–411 (1982).
15. R. Schreiber and H. B. Keller, 'Driven cavity flows by efficient numerical techniques', *J. Comput. Phys.*, **49**, 310–333 (1983).
16. K. Morgan, J. Periaux and F. Thomasset, *Analysis of Laminar Flow over a Backward Facing Step*, Vieweg, Braunschweig, 1984.
17. J. H. Morrison and M. Napolitano, 'Efficient solutions of two-dimensional incompressible steady viscous flows', *Comput. Fluids*, **16**, 119–132 (1988).
18. B. F. Armaly, F. Durst, J. C. F. Pereira and B. Schonung, 'Experimental and theoretical investigation of backward facing step flow', *J. Fluid Mech.*, **127**, 473–496 (1983).
19. Y. W. Ma, 'Investigation of numerical methods for solving the Navier–Stokes equations', *Math. Numer. Sinica*, **5**, 336–345 (1983).
20. S. C. R. Dennis and F. T. Smith, 'Steady flow through a channel with a symmetrical constriction in the form of a step', *Proc. R. Soc. Lond. A*, **372**, 393–414 (1980).
21. H. K. Moffatt, 'Viscous and resistive eddies near a sharp corner', *J. Fluid Mech.*, **18**, 1–18 (1964).
22. D. M. Hawken, P. Townsend and M. F. Webster, 'Numerical simulation of viscous flows in channels with a step', *Comput. Fluids*, **20**, 59–75 (1991).
23. A. Karageorghis and T. N. Phillips, 'Conforming Chebyshev spectral collocation methods for the solution of laminar flow in a constricted channel', *IMA J. Numer. Anal.*, **11**, 33–54 (1991).